Ion Beam Triangulation of Ultrathin Mn and CoMn Films Grown on Cu(001)

R. Pfandzelter, T. Bernhard, and H. Winter*

Institut für Physik, Humboldt-Universität zu Berlin, Invalidenstrasse 110, 10115 Berlin, Germany

(Received 8 May 2002; published 23 January 2003)

Total target currents for grazing scattering of keV protons from a crystal target are used to investigate the structure of surfaces and ultrathin films. This current shows pronounced maxima whenever the azimuthal incidence angle coincides with close-packed rows of atoms in the surface and subsurface layers. The real-space method is applied to study monolayer and bilayer films of Mn and of CoMn epitaxially grown on a Cu(001) surface.

DOI: 10.1103/PhysRevLett.90.036102 PACS numbers: 68.55.–a, 61.85.+p, 79.20.Rf

The understanding of physical and chemical properties of solid surfaces or ultrathin films requires a detailed knowledge of the geometrical arrangement of surface atoms. Powerful techniques for surface-specific analysis have been developed, such as scanning tunneling microscopy (STM), low-energy electron diffraction (LEED), or ion scattering; however, no all-purpose surface structural tool has emerged like x-ray diffraction for analysis of bulk structures [1]. While the surface symmetry is easily determined by LEED, a structure analysis involves considerable theoretical and computational effort, in particular, for large unit cells with many atoms. STM studies provide real-space images, but their interpretation in terms of surface structure is often a nontrivial task, since they represent contour maps of local electronic densities of states rather than positions of atoms.

In ion scattering, geometrical arrangements of atoms can be studied by making use of steering effects in the scattering of atomic particles along low-index crystallographic directions in the bulk and at surfaces of metals, semiconductors, and also insulators, i.e., scattering under channeling conditions [2]. The yield of backscattered ions is the most established probe in those studies [3,4]. In particular, low-energy ion beams with typically keV energies and an appropriate scattering geometry allow one to investigate the structure of solid surfaces by ion scattering spectroscopy [5]. Application of this technique is straightforward; however, instrumental requirements do not provide an easy integration into a standard setup for, e.g., surface physics related research.

In this Letter we propose a variant of ion scattering for studies on structures of surfaces and epitaxial ultrathin films. Light ions with energies in the keV range are scattered from the target surface under grazing angles of incidence typically some degrees, resulting in emission of target electrons [6], where the current of ejected electrons generally exceeds the current of incident ions [7–9]. When the ions impinge along a low-index crystallographic axis in the surface plane, they are steered by rows of surface atoms (''axial surface channeling'' [10]). The resulting projectile trajectories lead to a change in electron emission yields compared with ''random'' azimuthal settings. A variation of the target current as a function of the azimuthal angle of incidence thus exhibits structures for low-index directions [7–9].

As a consequence, the ''triangulation'' technique making use of ion beams provides direct information on periodic arrangements of atoms in the topmost layers of conducting surfaces. In the application of this method to studies on the structure of epitaxially grown ultrathin films, we can state the following attractive features:

(1) The experimental setup is simple, comprising an electrically insulated target on a rotatable manipulator and a collimated beam of light ions. The signal to noise ratio (target current) is high and can be recorded by a current meter. Requirements for the ion beam (energy, angular collimation, etc.) are modest, where beam energies of some tens of keV are favorable for good signals and angular resolution. In view of application, lower energies might be of interest, since compact keV ion guns are often attached to UHV chambers for sample cleaning.

(2) *In situ* and *real-time* analyses are possible, because grazing scattering geometry does not interfere with equipment for film growth. Fast ions are hardly subject to gas scattering and no secondary particles are detected, so that the topmost surface layer studies in (modest) gas pressure environments or at elevated temperatures become feasible.

(3) *At-sight* information on positions of atom cores is obtained, in particular, directions of close-packed atomic rows. No theoretical or computational data analysis is required. Thus, structures with large surface unit cells can be addressed, provided axial surface channeling can develop.

(4) Grazing scattering makes the technique surface specific. The surface sensitivity can be reduced by increasing the polar incidence angle of ion to the surface; i.e., studies of shallowly buried interfaces are accessible.

As examples for the application of this technique, we present studies on the structure of ultrathin Mn and CoMn films on a Cu(001) substrate. Based on LEED studies, Flores *et al.* [11] identified for growth of one and two monolayers (ML) of Mn on Cu(001) complex phases. A two-domain $c(8 \times 2)$ phase forms for deposition of a

monolayer at growth temperatures below 270 K. Capping of this layer by an additional Mn layer results in a two-domain $c(12 \times 8)$ diffraction pattern with substantial background. Both phases are metastable and rearrange into a $c(2 \times 2)$ structure upon heating.

The $c(2 \times 2)$ phase also forms upon deposition above 270 K. Experimental studies [12–16] on this $c(2 \times 2)$ phase show a surface alloy, where every other Cu atom is replaced by Mn atoms. A quantitative LEED analysis [11,17] of the $c(8 \times 2)$ phase points to a pure Mn topmost layer in a quasihexagonal arrangement. An analysis of the $c(12 \times 8)$ phase could not be performed due to the large size of the unit cell [11].

In our experiments, Mn is grown on the sputter-cleaned and annealed (001) surface of a Cu single crystal disk by electron beam evaporation. Growth is monitored by grazing scattering of 25 keV He atoms [18], where damped oscillations in the intensity of specularly reflected atoms indicate layer-by-layer growth with substantial film roughness. A sequence of LEED patterns $(1 \times 1) \rightarrow c(8 \times 2) \rightarrow c(12 \times 8)$ is observed at low temperatures and a $c(2 \times 2)$ pattern appears for room temperature growth. When the $c(8 \times 2)$ Mn phase is covered by a monolayer of Co from a second electron beam evaporator, a (1×1) pattern reemerges.

For ion beam triangulation of those phases, a beam of 25 keV protons is collimated by sets of slits and directed onto the target surface at a polar angle Φ to the surface plane and an azimuthal angle Θ to the [10] surface lattice direction {direction indices $[uv]$ refer to a square unit mesh with $\gamma = 90°$, as sketched in Fig. 1(a)}. The uncompensated target current is recorded during rotation of the target around its surface normal and normalized to the current measured at a highly transparent grid in the beam line in order to correct for beam current fluctuations.

The target current as a function of the azimuthal angle Θ at the clean Cu(001)-(1×1) surface is shown in Fig. 2 (top) for $\Phi = 1.6°$ and reveals pronounced maxima at eight nonequivalent low-index directions $[uv]$ in a square surface lattice. The current between maxima ("random orientation" stems from electron emission under "planar surface channeling,", i.e., for Φ smaller than a critical angle $\Phi_c = 2.5°$ [2], where protons are reflected from the topmost surface layer. When Θ corresponds to a low-index surface lattice direction, i.e., axial surface channeling, protons are steered by atomic rows, resulting in enhanced emission of electrons.

According to channeling theory, the critical angle for axial channeling Θ_c scales with $d[uv]^{-1/2}$ [2,8], $d[uv]$ being the interatomic spacing along rows. This explains the observation in Fig. 2 that peak widths in the target current decrease with $d[uv] = a\sqrt{u^2 + v^2}$ ($a = 2.55$ Å for Cu). Using screened interaction potentials [19], we calculate for Cu(001)-(1×1) base peak widths of $2 \times 6.0°$ and $2 \times 4.3°$ for the [10] and the [11] direction, respectively, in fair agreement with experiment [cf. Figs. 2 and 3, (insets)].

Figure 2 shows a comparison of target currents for Cu(001)-$c(8 \times 2)$-Mn (bottom) and Cu(001)-(1×1) (top). The curves show a mirror line of symmetry at 45°, consistent with square p- and two-domain rectangular c lattices observed by LEED. For $\Phi = 1.6°$, formation of the $c(8 \times 2)$ phase results in new peaks at $\Theta = 30°$ and 60°. The peaks at 0° and 90° retain high intensities, whereas other peaks of the (1×1) phase are substantially weakened. Thus, peaks at 0°, 30°, 60°, and 90° are attributed to the $c(8 \times 2)$ Mn film layer (Fig. 2, shaded peaks), whereas the residual curve shows the characteristics of the (1×1) Cu substrate. This assignment of peaks is confirmed by measurements for $\Phi = 2.5°$ (Fig. 2, thin curves). Owing to the larger incidence angle ($\Phi \approx \Phi_c$), protons penetrate into deeper layers; i.e.,

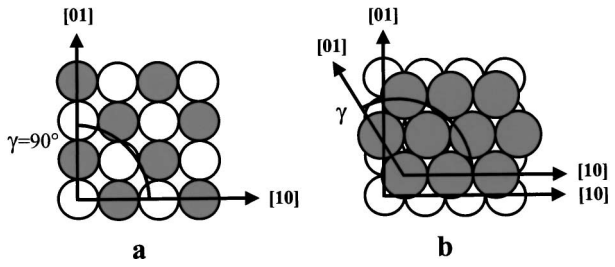

FIG. 1. Structural model for a $c(2 \times 2)$ MnCu surface alloy (a) and a $c(8 \times 2)$ (quasi)hexagonal Mn layer on Cu(001) (one domain) (b). White circles: Cu; black circles: Mn.

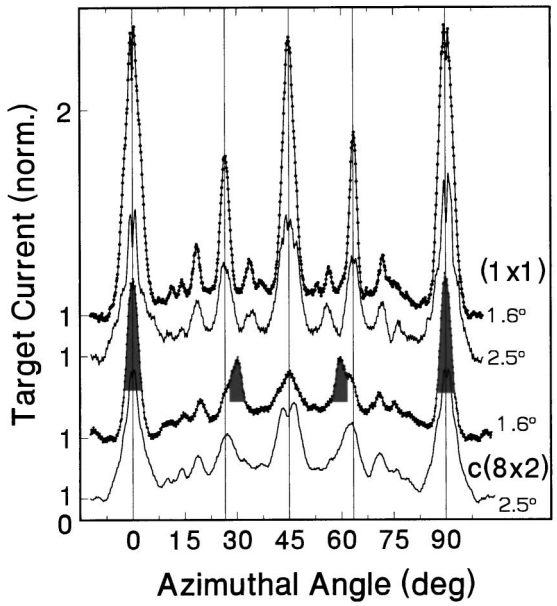

FIG. 2. Target current (normalized, with offsets) versus azimuthal angle of incidence Θ for 25 keV protons scattered from Cu(001)-(1×1) (top) and Cu(001)$c(8 \times 2)$-Mn (bottom) under Φ as indicated. Peaks owing to the Mn overlayer are shaded, major peaks owing to the Cu substrate are marked by vertical lines.

buried layers contribute to the signal and overlayer peaks are weak.

Regular 30° intervals between close-packed atomic rows imply a hexagonal arrangement of film atoms with [10] ‖ [10] orientation between hexagonal film and cubic substrate lattice {direction indices $[uv]$ for the film refer to a hexagonal unit mesh as sketched in Fig. 1(b)}. 0° and 60° peaks belong to $c(8 \times 2)$ domains and 30° and 90° peaks to $c(2 \times 8)$ domains. The large width of the 45° peak at $\Phi = 1.6°$ and its bimodal shape at $\Phi = 2.5°$ (Fig. 2) suggest a superposition of the 45°-substrate peak and nearby overlayer peaks. We note that a slight reduction of the angle between hexagonal unit vectors from $\gamma = 120°$ to 119.7° required to form a commensurate lattice [17] cannot be resolved.

Figure 3 shows a compilation of target currents at $\Phi = 1.6°$ for (from top to bottom) Cu(001)-(1×1), Cu(001)-$c(2 \times 2)$-Mn, an incompletely developed Cu(001)-$c(8 \times 2)$-Mn (transition), Cu(001)-$c(8 \times 2)$-Mn, Cu(001)-$c(12 \times 8)$-Mn, and Cu(001)-(1×1)-Mn-Co. As to angular positions of peaks, the curve for the $c(2 \times 2)$ phase is a replica of the curve for clean Cu(001), indicating a square lattice of the film layer. The substantially lower peak intensities are ascribed to film roughness. A rough surface mediates penetration of protons into the surface, which leads to an overall increase of the target current. Incidentally, this may also be the reason for the convex shape of the current for random orientation. For substrate steps running preferentially along ⟨10⟩ directions, the (projected) step density encountered by protons is maximal at $\Theta = 45°$.

Inspection of peak widths for $c(2 \times 2)$ shows a reduction by a factor of about $1/\sqrt{2}$ along [10] ($\Theta = 0°$), whereas the width along [11] (45°) does not change for the $(1 \times 1) \rightarrow c(2 \times 2)$ transition (Fig. 3 insets). This implies a doubling of the interatomic spacing d[10], whereas d[11] is not changed. This is consistent with a large buckling in the $c(2 \times 2)$ surface alloy, where Mn atoms are displaced outwards with respect to Cu atoms [12] [see Fig. 1(a)]. We calculate base widths of $2 \times 4.3°$ and $2 \times 4.9°$ for the [10] and [11] directions, respectively, consistent with experiment (Fig. 3 insets).

Low-temperature deposition of submonolayer amounts of Mn leads to an incompletely developed $c(8 \times 2)$ phase with weak hexagonal peaks in the target current (Fig. 3, curve labeled transition). Upon completion of the monolayer, overlayer peaks gain intensity, whereas substrate peaks are reduced.

Deposition of a second monolayer of Mn on top results in the formation of a $c(12 \times 8)$ phase with a substantially different target current, indicating a new structure for *both* film layers. In addition to the strong peak at 0° (90°), peaks appear at $20.8° \pm 0.7°$, $34.3° \pm 0.3°$, $55.2° \pm 0.2°$, and $69.4° \pm 0.6°$, whereas the peak at 45° is further reduced and seems to be split. Measurements at a reduced incidence angle $\Phi = 1.0°$ (Fig. 3, grey curve) show an increase of the peak at 20.8° and a decrease of the peak at

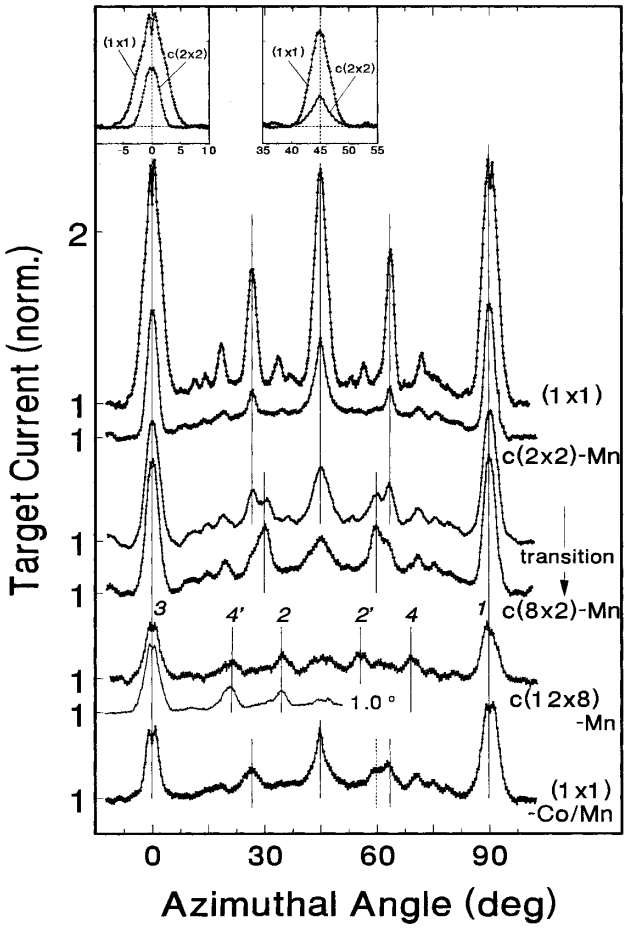

FIG. 3. Target current (normalized, with offsets) versus Θ for 25 keV protons scattered under $\Phi = 1.6°$ from Cu(001)-(1×1), Cu(001)-$c(2 \times 2)$-Mn, incomplete Cu(001)-$c(8 \times 2)$-Mn ("transition"), Cu(001)-$c(8 \times 2)$-Mn, Cu(001)-$c(12 \times 8)$-Mn, and Cu(001)-(1×1)-Mn-Co (from top to bottom). Vertical lines indicate close-packed surface lattice directions. Numbered peaks for $c(12 \times 8)$ correspond to directions indicated in Fig. 4. The grey curve is the target current for proton scattering from Cu(001)-$c(12 \times 8)$-Mn under $\Phi = 1.0°$. Insets: Peaks along the [10] and [11] directions for Cu(001)-(1×1) and Cu(001)-$c(2 \times 2)$-Mn, respectively.

34.3°. In view of the higher surface sensitivity for small incidence angles, we thus assign peaks at 0°, 20.8°, and 69.4° to the surface layer, whereas peaks at 0°, 34.3°, and 55.2° stem from the interface layer. The latter angles correspond, within experimental uncertainty, to diagonal lines of $c(12 \times 8)$ or $c(8 \times 12)$ unit cells (33.7° or 56.3°, respectively). This indicates a two-domain distorted hexagonal arrangement for Mn atoms at the interface, where unit vectors enclose an angle of 112.6° and are aligned along diagonal lines of the $c(12 \times 8)$ unit cell [Fig. 4(a)].

The coverage of this interface layer is larger (1.02 ML) than the coverage of the $c(8 \times 2)$ film (0.875 ML). This is plausible in view of strong magnetovolume effects characteristic for Mn [20]. Larger coordination number and increased Mn d-d hybridization in the interface layer

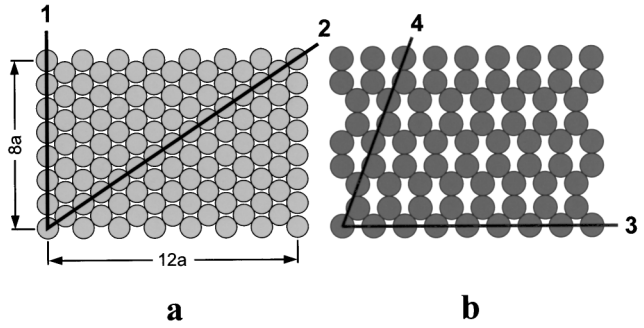

FIG. 4. Structural model (one domain) for a $c(12 \times 8)$ Mn bilayer on Cu(001). (a) Interface layer; (b) surface layer. Grey and black circles: Mn.

tend to reduce magnetic moments of Mn atoms, resulting in a more densely packed film.

Peaks at 20.8° and 69.4° indicate that close-packed rows within the surface layer are aligned along diagonal lines of (8×3) or (3×8) cells (20.6° or 69.4°, respectively). This is consistent with a $c(12 \times 8)$ symmetry and an arrangement of atoms as proposed in Fig. 4(b), where one domain corresponding to a coverage of 2/3 ML is shown.

We also present in Fig. 3 data obtained after deposition of one monolayer of Co on top of the $c(8 \times 2)$ Mn phase. This results in a rearrangement into a (1×1) pseudomorphic structure, in agreement with our LEED study. This structure extends over *both* film layers, although patches with $c(8 \times 2)$ structure seem to survive (Fig. 3, dashed line), presumably due to incomplete wetting of the Mn monolayer.

In our experiments we used proton beams, where radiation damage of the films is negligible, as checked by high dose (10^{15} ions cm^{-2}) irradiation experiments. It is appealing to combine the technique with intended irradiation effects, e.g., recoil of film atoms in collisions with heavy ions, because momentum transfer in grazing ion surface scattering should be predominantly within the film plane [21], favoring controlled structural, topographical, or compositional changes of ultrathin films. Tests for grazing scattering of 25 keV He^+ ions from Cu(001)-$c(8 \times 2)$-Mn show that target currents gradually change from the $c(8 \times 2)$ to a (1×1) structure. This transition occurs at a dose of about $3 \cdot 10^{14}$ ions cm^{-2}, where sputter effects are of minor importance, as checked by Auger electron spectroscopy. Note that the phase diagram for Cu(001)-Mn does not reveal a (1×1) structure for monolayer films, i.e., the structure is induced by energy transfer in collisions with He^+ ions.

In conclusion, we propose ion beam triangulation as a powerful real-time technique to analyze the arrangement of atoms at surfaces and ultrathin films. Application of the technique to monolayer and bilayer films of Mn and of CoMn on Cu(001), partly with structures that have not been resolved to date, shows that essential structural information is obtained from a straightforward analysis of data. In particular, target current measurements reveal *at-sight* information on directions of closed-packed atomic rows at the surface. Apart from studies of structures with large unit cells, promising applications of the technique are real-time characterizations of the evolution of atomic structures during growth processes or phase transitions and a combination with ion beam assisted deposition and modification of films.

Helpful discussions with Dr. M. Grüne (Bonn) are gratefully acknowledged. This work was supported by the Deutsche Forschungsgemeinschaft (Sonderforschungsbereich 290).

*Electronic address: winter@physik.hu-berlin.de

[1] D. P. Woodruff, Surf. Sci. **500**, 147 (2002).
[2] D. S. Gemmell, Rev. Mod. Phys. **46**, 129 (1974).
[3] L. C. Feldman, J. W. Mayer, and S. T. Picraux, *Materials Analysis by Ion Channeling* (Academic Press, New York, 1982).
[4] J. F. van der Veen, Surf. Sci. Rep. **5**, 199 (1985).
[5] H. Niehus, W. Heiland, and E. Taglauer, Surf. Sci. Rep. **17**, 213 (1993).
[6] R. A. Baragiola, E. V. Alonso, and A. Oliva Florio, Phys. Rev. B **19**, 121 (1979).
[7] H. J. Andrä, H. Winter, R. Fröhling, N. Kirchner, H. J. Plöhn, W. Wittmann, W. Graser, and C. Varelas, Nucl. Instrum. Methods **170**, 527 (1980).
[8] H. Winter, Ph.D. thesis, Universität München, 1986 (author not identical with last author of this Letter).
[9] M. Hasegawa, K. Kimura, Y. Fujii, M. Suzuki, Y. Susuki, and M. Mannami, Nucl. Instrum. Methods Phys. Res., Sect. B **33**, 334 (1988).
[10] R. Sizmann and C. Varelas, Nucl. Instrum. Methods **132**, 633 (1976).
[11] T. Flores, M. Hansen, and M. Wuttig, Surf. Sci. **279**, 251 (1992).
[12] M. Wuttig, Y. Gauthier, and S. Blügel, Phys. Rev. Lett. **70**, 3619 (1993).
[13] R. G. P. van der Kraan and H. van Kempen, Surf. Sci. **338**, 19 (1995).
[14] R. Toomes, A. Theobald, R. Lindsay, T. Geissel, O. Schaff, R. Didszhun, D. P. Woodruff, A. M. Bradshaw, and V. Fritzsche, J. Phys. Condens. Matter **8**, 10231 (1996).
[15] D. Brown, T. C. Q. Noakes, D. P. Woodruff, P. Bailey, and Y. Le Goaziou, J. Phys. Condens. Matter **11**, 1889 (1999).
[16] S. D'Addato and P. Finetti, Surf. Sci. **471**, 203 (2001).
[17] Y. Gauthier, M. Poensgen, and M. Wuttig, Surf. Sci. **303**, 36 (1994).
[18] R. Pfandzelter, T. Igel, and H. Winter, Phys. Rev. B **62**, R2299 (2000).
[19] D.J. O'Connor and J.P. Biersack, Nucl. Instrum. Methods Phys. Res., Sect. B **15**, 14 (1986).
[20] M. Eder, J. Hafner, and E. G. Moroni, Phys. Rev. B **61**, 11 492 (2000).
[21] P. M. DeLuca, K. C. Ruthe, and S. A. Barnett, Phys. Rev. Lett. **86**, 260 (2001).